Smart Structures and Systems, *Vol. 14, No. 6 (2014) 1005-1030*
DOI: http://dx.doi.org/10.12989/sss.2014.14.6.1005

A novel hybrid testing approach for piping systems of industrial plants

Oreste S. Bursi*, Giuseppe Abbiati[a] and Md S. Reza[b]

Department of Civil, Environmental and Mechanical Engineering, University of Trento, Via Mesiano 77, 38123, Trento, Italy

(Received May 30, 2014, Revised August 20, 2014, Accepted August 30, 2014)

Abstract. The need for assessing dynamic response of typical industrial piping systems subjected to seismic loading motivated the authors to apply model reduction techniques to experimental dynamic substructuring. Initially, a better insight into the dynamic response of the emulated system was provided by means of the principal component analysis. The clear understanding of reduction basis requirements paved the way for the implementation of a number of model reduction techniques aimed at extending the applicability range of the hybrid testing technique beyond its traditional scope. Therefore, several hybrid simulations were performed on a typical full-scale industrial piping system endowed with a number of critical components, like elbows, Tee joints and bolted flange joints, ranging from operational to collapse limit states. Then, the favourable performance of the L-Stable Real-Time compatible time integrator and an effective delay compensation method were also checked throughout the testing campaign. Finally, several aspects of the piping performance were commented and conclusions drawn.

Keywords: pseudo-dynamic test; real-time test; model reduction; coupled system; piping system

1. Introduction

1.1 Background and motivation

Hybrid simulations, such as Pseudo-Dynamic (PDT) and Real time (RT) Testing with Dynamic Substructuring (DS) (Mahin and Shing, 1985, Shing *et al.* 1996, Saouma and Sivaselvan 2008, Bursi and Wagg 2008) define experimental techniques; there, the overall response of an emulated system is evaluated by combining the experimental response of a Physical Substructure (PS) -which is generally the most critical part of a system/structure- with the numerical response of a Numerical Substructure (NS). Thus, these methods permit testing of a structure, essentially without a size limit, by the use of actuators, controllers and standard computers.

These experimental methods were successfully used in testing various mechanical systems (Melo *et al.* 2001, Bursi *et al.* 2008, 2011, Horiuchi *et al*. 1999, Wallace *et al.* 2007) including civil structures (Braconi *et al.* 2008a, b, Chrysostomou *et al*. 2013). Unlike a RT, which is carried

*Corresponding author, Professor, E-mail: oreste.bursi@unitn.it
[a] Ph.D. Student, E-mail: giuseppe.abbiati@unitn.it
[b] Postdoc Researcher, E-mail: md.shahin.reza@unitn.it

http://www.techno-press.org/?journal=sss&subpage=8 ISSN: 1738-1584 (Print), 1738-1991 (Online)

out at real time, a PDT is performed at an extended time scale, typically 50-200 times slower than the actual earthquake time, requiring inertia and damping forces to be numerically modelled. However, since rate dependent effects can practically be neglected for steel components (Yoshihiko 2012), a PDT can also potentially reproduce their actual responses under dynamic loading. In the case of simple structural topologies, i.e., shear type frames, inverted pendulum systems, chain like systems, etc., few actuators handling the totality of physical Degrees of Freedom (DoFs) can efficiently reproduce the response path of tested specimens; and the system of equations of motion can be solved through suitable time integrators. Nonetheless, this approach is not suitable for dealing with complex PSs subjected to distributed inertia forces, where a plenty of physical DoFs come on stage; and this is the case of typical piping networks.

In greater detail, piping systems play a highly important role in many industries, such as petrochemical, oil and gas and nuclear plants, and a single failure can trigger serious accidental chains. As a result, after the Fukushima earthquake (Vervaeck and Daniell 2012), Standards for special risk plants greatly increased the importance factor γ_I to be applied to design Peak Ground Acceleration (PGA). See, for instance, the value of $\gamma_I \approx 2$ imposed in France (Ministere 2011). Therefore, a special attention to ensure their safe operations represents an imperative requirement. Nevertheless, these systems, comprising elbows, Tee joints and flange joints as well as support structures, suffered significant damages during recent earthquakes causing severe losses both to human lives and to the environment (Krausmann *et al.* 2010, Zare and Wilkson 2010, Paolacci *et al.* 2013a). This led researchers to carry out considerable studies on the seismic safety assessment of piping systems and their components (Touboul *et al.* 2006, Reza *et al*. 2013). However, so far only few experimental investigations -mainly through shaking table tests- have been performed on such structures at full-scale under realistic seismic loading (DeGrassi *et al.* 2008, Otani *et al.* 2011).

The potential usefulness of hybrid simulation techniques for assessing dynamic behaviour of typical industrial piping networks subjected to realistic seismic loading motivated the authors to shed light on model reduction techniques applied to coupled systems. Thus, the applicability range of experimental dynamic sub structuring was enhanced.

1.2 Scope

A number of model reduction techniques applied to hybrid coupled systems is presented and discussed in this paper. As a result, several PDT and RT were conducted on the aforementioned piping system –or emulated system- under different levels of seismic loading, corresponding to both serviceability and ultimate limit states for the supporting structure suggested by Italian performance-based earthquake engineering standards (Norme Techniche 2008). Hence, the work presented in this study enabled model reduction to PSs characterized by distributed loads and a large number of DoFs, where just a subset of them at the interconnections, was handled by means of actuators.

In detail, the paper is organized as follows. Initially, the case study as well as the selection of seismic inputs were described. Then, Finite Element (FE) modelling of the piping system and its critical components, such as elbows, were presented. According to time history analyses conducted on the aforementioned FE model, the tailoring of the PS was then presented and a modified FE model embedding the actual coupling conditions was introduced as reference, for the validation of interconnections. Before introducing any reduction strategy, a clear insight into the dynamic response of the emulated system from the PS perspective was provided. In detail, the Principal

Component Analysis (PCA) was applied to time history data sets made of displacement responses of physical DoFs of the piping system. The state space path followed by the specimen was traced and reduction basis requirements established. Accordingly and complying with experimental limitations of each testing strategy, consistent reduction bases were defined for both PDT and RT techniques in the case of an elastic response of the PS. Successively, a Modified version of the System Equivalent Reduction-Expansion Process (M-SEREP) (O'Callahan *et al*. 1989b) and Craig-Bampton reduction methods (Craig and Bampton 1968) were employed for the reduction of both the PS and distributed earthquake forces. This allowed for an effective experimental testing of the actual system.

With regard to time integration, the L-Stable Real Time compatible (LSRT2) (Bursi *et al*. 2008, 2011) was employed, together with an effective delay compensation method (Wu *et al*. 2013). Successively, relevant implementations and experimental results were shown. Finally, conclusions were drawn and future perspective offered.

2. A distributed parameters piping system

2.1 Main characteristics and dimensions

A typical full-scale industrial piping system placed on a steel support structure, as illustrated in Fig. 1(a), was investigated within this study; its general dimensions and other geometrical properties depicted in Fig. 1(b) were taken after DeGrassi *et al.* (2008). The piping network contained 8" (outer dia: 219.08 mm; thickness: 8.18 mm) and 6" (outer dia: 168.28 mm; thickness: 7.11 mm) schedule 40 straight pipes and several critical components, i.e., elbows, a Tee joint and an EN 1092-1 standard PN 40 weld-neck bolted flange joint. The pipes were of API 5L Gr. X52 material (nominal f_y and f_u equal to 418 MPa and 554 MPa, respectively) and were filled with water at an internal pressure of 3.2 MPa, corresponding to 80% of the maximum allowable pressure of the piping network.

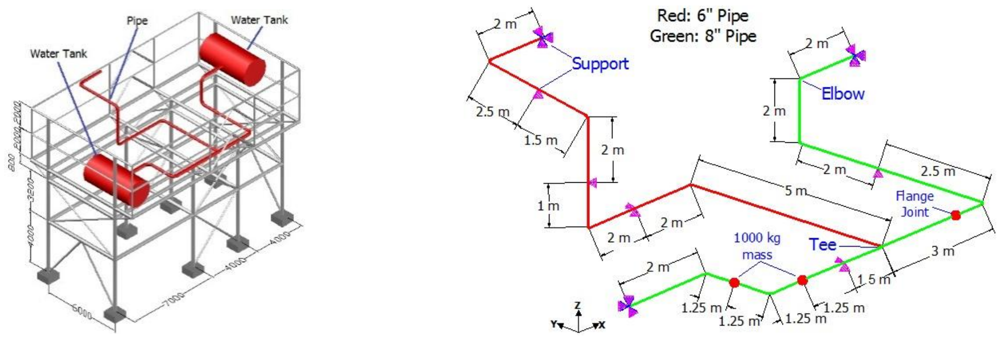

(a) (b)

Fig. 1 (a) A 3D model of the piping system placed on the support structure and (b) specifications and dimensions of the piping system after DeGrassi *et al.* (2008). Dimensions are in mm

2.2 Selection of input earthquake loading

The piping network was placed on a steel support structure shown in Fig. 1(a) that typically acts as a dynamic filter; it causes amplifications of input earthquakes at different structure locations. Therefore, to select realistic earthquake input loadings, earthquake accelerations were generated on elevated floors of the support structure through time history analyses carried out by means of an FE model of the structure subjected to a base input, i.e., a natural accelerogram taken from the European Strong-motion Database (ESD, http://www.isesd.hi.is/ESD_Local/frameset.htm). A reference floor accelerogram was thus chosen; it was the most severe floor accelerogram in terms of amplitude and resonance frequency of the piping network with a relevant PGA at about 4.13 m/s^2. To comply with performance-based earthquake engineering Italian Standards (NormeTechniche 2008), its PGA was magnified corresponding to both serviceability (operational- SLO, damage –SLD) and ultimate limit states (safe life –SLV, collapse -SLC) of the support structure as listed in Table 1.

As can be appreciated in Fig. 2(b), the period T at maximum amplification was around 0.2 sec, which was close to the natural frequency of the piping system.

Table 1 PGAs corresponding to Serviceability and Ultimate Limit States of support structure

Limit States			PGA (m/s^2)	PGA (g)
Serviceability Limit states	SLO	Operational limit state	0.77	0.08
	SLD	Damage limit state	1.1	0.11
Ultimate Limit States	SLV	Safe life limit state	4.13	0.42
	SLC	Collapse limit state	5.88	0.60

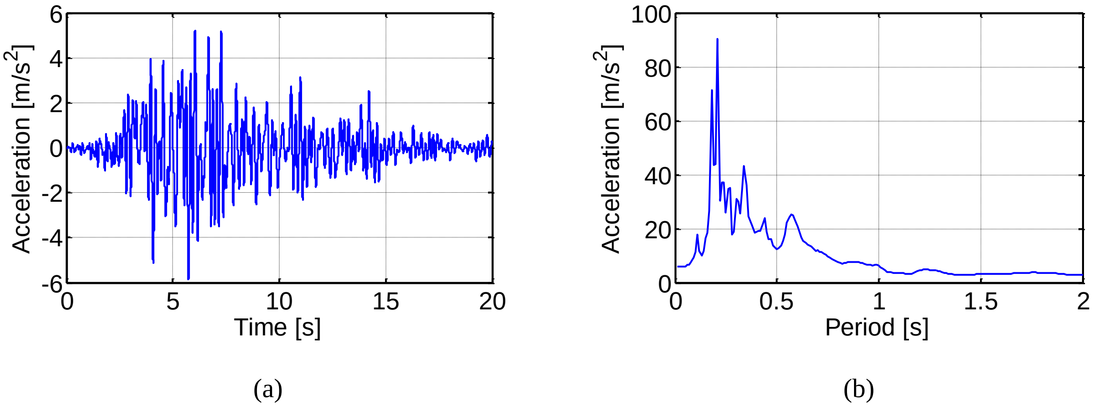

Fig. 2 (a) SLC reference floor accelerogram and (b) relevant acceleration response spectrum for 0.5% equivalent viscous damping

2.3 FE modelling and analysis

In order to perform preliminary numerical analyses and to extract system matrices for hybrid simulations, a 3D FE model of the piping system was developed in ANSYS (2007). All pipes including elbows were modelled using straight beam elements with pipe sections. Two 1000 kg masses, employed to take into account valves, etc., were connected to two relevant joints through MASS21 elements. Pipe material density was increased to take into account water mass.

Flexible elbow components represent potential critical locations in a piping network where stresses are intensified owing to their geometrical irregularity; see, in this respect, Fig. 3 where unsymmetrical cyclic responses of pipe elbows obtained from tests carried out by Varelis *et al*. (2012) are depicted. To consider their elastic behaviour in the FE model, flexibilities of straight elbow elements (EN 13480-3, 2002) were adjusted according to an ABAQUS-based FE SHELL model (Hibbit *et al*. 2003). In greater detail, original curved elbow elements were modelled in ABAQUS software and 3D FE analyses under axial, shear and bending loading were performed; see in this respect Fig. 4, where in-plane and out-of-plane moment-rotation curves of an elbow element obtained from FE analyses are presented. Thus, an equivalence between ABAQUS SHELL FE curved and ANSYS straight elastic elements was established. Each elbow had a radius R equal to 1.5 times the outer diameter d_{out} of connecting pipes; moreover, the flexibility effect of an elbow was considered to spread across a distance equal to two times the mean diameter of the pipe; the equivalent straight elbow element consisted of a curved and two straight parts; their individual flexibilities were added to obtain the overall flexibility of the straight element.

In this view, elastic stiffness matrices of equivalent straight elbows were developed according to the Euler-Bernoulli (EB) beam theory. In particular, the stiffness matrix of a straight elbow element based on the EB theory can be expressed in the following form

$$\begin{bmatrix} k_{11} & 0 & 0 & k_{14} & 0 & 0 \\ 0 & k_{22} & k_{23} & 0 & k_{25} & k_{26} \\ 0 & k_{32} & k_{33} & 0 & k_{35} & k_{36} \\ k_{41} & 0 & 0 & k_{44} & 0 & 0 \\ 0 & k_{52} & k_{53} & 0 & k_{55} & k_{56} \\ 0 & k_{62} & k_{63} & 0 & k_{65} & k_{66} \end{bmatrix} \begin{bmatrix} u_1 \\ v_1 \\ \varphi_1 \\ u_4 \\ v_4 \\ \varphi_4 \end{bmatrix} = \begin{bmatrix} H_1 \\ F_1 \\ M_1 \\ H_4 \\ F_4 \\ M_4 \end{bmatrix} \quad \begin{aligned} & k_{11} = k_{44} = -k_{14} = -k_{41} = K_{ax} \\ & k_{22} = k_{55} = -k_{25} = -k_{52} = K_{sh} \\ & k_{33} = k_{66} = K_{bg} \\ & k_{36} = k_{63} = (1-\omega)\frac{1}{6}K_{sh}l^2 + \omega\frac{1}{2}K_{bg} \\ & -k_{23} = -k_{32} = -k_{26} = k_{35} = k_{53} = -k_{62} = k_{56} = k_{65} = (1-\omega)\frac{1}{2}K_{sh}l + \omega\frac{3}{2}\frac{K_{bg}}{l} \end{aligned} \tag{1}$$

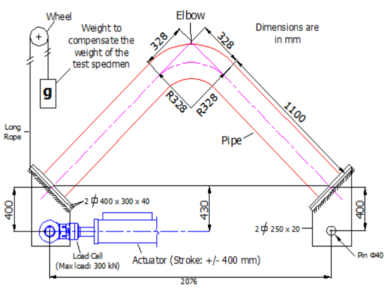

(a)

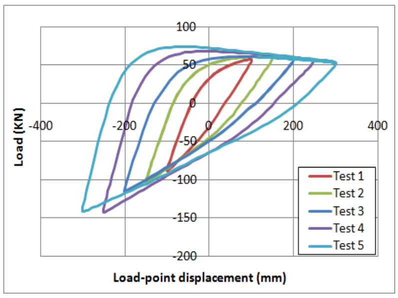

(b)

Fig. 3 Experiments on pipe elbows performed by Varelis *et al.* (2012): (a) test set-up and (b) cyclic response where only in-plane contributions are shown for simplicity. In (1), u and v are displacements; φ is rotation; H and F are forces; M is moment; $\boldsymbol{K_{ax}}, \boldsymbol{K_{s}}$ **and** $\boldsymbol{K_{bg}}$ are axial, shear and bending stiffness coefficients, respectively. By varying the elbow thickness, the elastic stiffness of each straight elbow was fitted with those found from the above-mentioned analyses. An optimal value of ω = 0.89 was found and out of plane bending and shear were also considered in these analyses. The adjusted geometry and properties of modified straight elbow elements are reported in Table 2.

3. Substructuring

For sub structuring purposes, the piping system was divided into two parts: (i) a PS, which was physically built in the lab and loaded through actuators; (ii) a NS that was solved via software; the two substructures exchanged information through coupling DoFs they mutually shared. Since physical excitation of rotational DoFs is very difficult to accomplish (Klerk *et al.* 2008), coupling nodes with bending moment close to zero in the xy plane -most of the pipes run in this plane- were selected; see Fig. 5(a) in this respect. Accordingly, two MOOG actuators were attached to those nodes and were oriented in x direction. Moreover, Fig. 5(b) illustrates the important node numbering of two substructures and relevant boundary conditions.

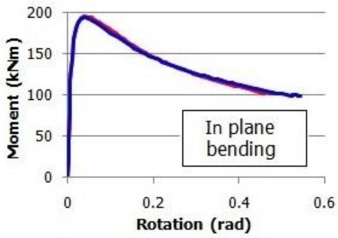

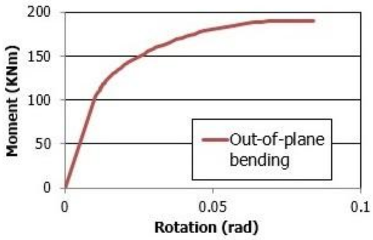

Fig. 4 In-plane and out-of-plane moment-rotation relationships of elbow under bending loading from ABAQUS FE analyses

Table 2 Elbow properties considered in the piping system model with straight elements

Property	8" Elbow		6" Elbow	
	Original	Modified	Original	Modified
Outer diameter (mm)	219.08	219.08	168.28	168.28
Thickness, e_n (mm)	8.18	6.61	7.11	4.35
Flexibility factor, k_B	6.84	1.35	5.97	2.46
Moment of inertia, J (mm^4)	3.02×10^7	2.49×10^7	1.17×10^7	7.53×10^6

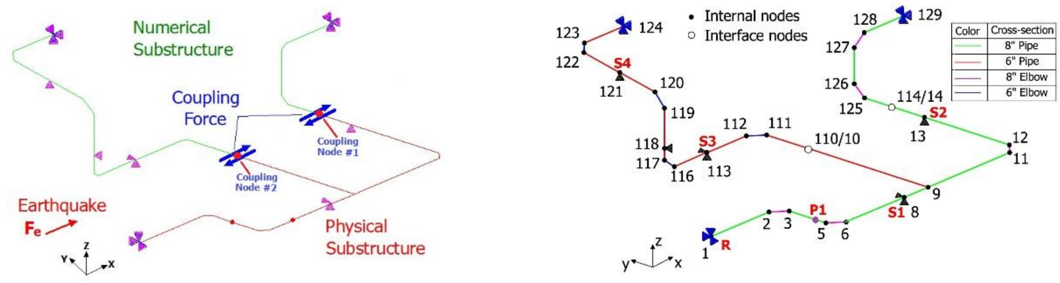

(a) (b)

Fig. 5 (a) PS, NS and relevant coupling nodes and (b) Schematic of the FE model of the piping system showing pipe sections and significant nodes

In detail, the following coupling conditions were forced for translational and rotational DoFs, respectively

$$u_x^N = u_x^P,\ u_y^N = u_y^P = 0,\ u_z^N = u_z^P = 0 \tag{2}$$

$$\theta_x^N \neq \theta_x^P,\ \ \theta_y^N \neq \theta_y^P,\ \ \theta_z^N \neq \theta_z^P \tag{3}$$

where, u and θ represents displacements and rotations, respectively; N and P refers to the NS and PS, respectively. Eqs. (2) and (3) show that the two coupling nodes were constrained to move in the x direction, thus satisfying compatibility conditions. Rotations were kept free while movements along y and z were constrained. Therefore, hybrid tests were conducted by means of two hydraulic actuators which imposed displacement commands in the x direction of the PS.

A careful reader can note that the support structure depicted in Fig. 1(a) was not included in the NS for two reasons: i) to impart the most severe earthquake in terms of PGA, amplitude and frequency to the piping system; ii) to avoid the complexity of a non-linear computation of the NS during RT. In this respect, the floor of the support structure that sustained the piping network was considered as a rigid floor. In fact, a seismic analysis of the supporting structure with the piping system exhibited that the maximum Root Mean Square (RMS) between relative movements of support points S1, S2, S3 and S4 with respect to the reference point R, see Fig. 5(b), was about 0.83 mm. This value was assumed to be small compared to the RMS of the maximum relative displacement of piping system points, i.e., 50.87 mm at point P1; see again Fig. 5(b). As a result, the assumption of rigid floor was justified. Moreover as presented in Subsection 2.2, the input earthquake for experiments was chosen to be the most severe floor accelerogram in terms of amplitude and resonance frequency of the piping network among the ones at support points. Finally without inelastic support structure, the earthquake amplification at the floor level both at the SLV and SLC limit states was not reduced.

3.1 Substructuring FE modelling

In order to validate dynamic substructuring, an additional ANSYS FE model embedding the actual coupling conditions of Eqs. (2) and (3), was developed. This model, defined as the ANSYS

Reference Model (RM), was assumed as the reference for validating model reduction techniques, time-integration algorithms as well as the experimental set-up. The RM in which both substructures PS and NS were embedded was compared with the ANSYS FE model of the actual piping system, referred herein as the Continuous Model (CM); there, the full coupling between both rotational and translational interface DoFs is enforced; hence the name "Continuous". Modal analyses conducted on both the CM and RM proved the effectiveness of the coupling setting, which slightly affected the dynamic properties of the piping network. In particular in both cases, the first 10 modes were able to excite about 80% of the total mass of the piping system in the x direction, as reported in Table 3.

For both models, Mode #1 and Mode #2 depicted in Fig. 6 carried most of the modal mass. They were the basis for the calculation of the equivalent viscous damping according to a Rayleigh formulation.

Table 3 First 10 eigenfrequencies and participation masses of the piping system model

	ANSYS CM		ANSYS RM	
Mode	Frequency [Hz]	Modal mass ration	Frequency [Hz]	Modal mass ration
1	6.0213	0.3235	5.8666	0.2413
2	6.5427	0.2546	6.4731	0.3359
3	7.1418	0.0005	7.0579	0.0000
4	8.2225	0.0050	7.4108	0.0060
5	9.7197	0.0584	9.5757	0.0518
6	12.0349	0.0578	11.9818	0.0771
7	13.0057	0.0357	12.4471	0.0276
8	15.1504	0.0001	14.8247	0.0000
9	17.8459	0.0795	15.3468	0.0089
10	18.5989	0.0175	17.4335	0.0593
	TOTAL	0.8327	TOTAL	0.8078

(a) (b)

Fig. 6 (a) Mode #1 at 5.87Hz and (b) Mode #2 at 6.47Hz of the ANSYS RM.

An additional comparison between RM and CM FE models was made based on the Modal Assurance Criterion (MAC), which is a score aimed at comparing two eigenvectors (Pastor *et al*. 2012). In detail, a MAC matrix can compare eigenvectors of two models and provides a unit value for perfect correlation and zero for orthogonal modes. It is defined as follows

$$MAC(\phi_{CM}, \phi_{RM}) = \frac{\left(\phi_{CM}^T \phi_{RM}\right)^2}{\left(\phi_{CM}^T \phi_{RM}\right) \cdot \left(\phi_{RM}^T \phi_{RM}\right)} \tag{4}$$

where ϕ_{CM} and ϕ_{RM} are eigenvectors of CM and RM, respectively. The relevant components of the MAC matrix are reported in Table 4. A careful reader can observe that the two main modes of the piping system, i.e., Mode #1 and Mode #2, agree with a MAC value greater than 0.92.

Further time history analyses were conducted on both the CM and the RM. Relevant differences were measured by the Normalized Energy Error (NEE) and the Normalized Root-Mean Square Error (NRMSE) defined as

$$\text{NEE} = \left| \frac{\sum_{i=1}^{n} x_{RM,i}^2 - \sum_{i=1}^{n} x_{CM,i}^2}{\sum_{i=1}^{n} x_{CM,i}^2} \right| \tag{5}$$

$$\text{NRMSE} = \frac{\sqrt{\sum_{i=1}^{n} \frac{\left(x_{RM,i} - x_{CM,i}\right)^2}{n}}}{\max\left(\mathbf{x}_{CM}\right) - \min\left(\mathbf{x}_{CM}\right)} \tag{6}$$

Table 4 MAC matrix between ANSYS CM and RM models

		ANSYS RM									
		1	2	3	4	5	6	7	8	9	10
ANSYS CM	1	**0,94**	0,10	0,00	0,03	0,00	0,00	0,02	0,00	0,00	0,04
	2	0,26	**0,92**	0,00	0,03	0,00	0,03	0,02	0,00	0,01	0,02
	3	0,00	0,00	**0,92**	0,07	0,00	0,00	0,00	0,05	0,00	0,00
	4	0,01	0,01	0,01	**0,86**	0,00	0,02	0,08	0,00	0,00	0,01
	5	0,00	0,00	0,00	0,10	**0,93**	0,01	0,04	0,00	0,00	0,00
	6	0,00	0,02	0,00	0,00	0,00	**0,88**	0,00	0,00	0,02	0,00
	7	0,02	0,01	0,00	0,02	0,00	0,14	**0,88**	0,00	0,00	0,02
	8	0,00	0,00	0,06	0,00	0,00	0,00	0,00	**0,97**	0,00	0,00
	9	0,05	0,02	0,00	0,02	0,02	0,00	0,00	0,00	**0,01**	0,86
	10	0,00	0,02	0,00	0,01	0,00	0,03	0,01	0,03	0,66	**0,02**

Table 5 NRMSE and NEE between RM and CM

Error Measure	Coupling DoF #1	Coupling DoF #2
NEE	0.085	1.548
NRMSE	0.099	0.214

where, $\boldsymbol{x_{CM}}$ and $\boldsymbol{x_{RM}}$ are nodal displacement responses of CM and RM, respectively; n is the relevant length of samples. In detail, NEE involves the signal energy, and is significantly sensitive to amplitude differences and less sensitive to frequency mismatches. The NRMSE, on the other hand, shows high sensitiveness to frequency variation and is little affected by amplitude differences. Both normalizations are such that the amplitude -PGA value- of the seismic input has no effects on both NEE and NRMSE in the linear range. With regard to coupling DoFs shown in Fig. 5, Table 5 reports values of the aforementioned errors.

Both error values highlight a comparatively less accuracy on Coupling DoF #2. In fact, a preliminary seismic time history analysis of the CM exhibited that bending moments, which were closed to zero in coupling nodes, were higher in Coupling Node #2 than Coupling Node #1. Since these moments were neglected for substructuring purposes, Coupling Node #2 was more affected by this approximation. Nonetheless, as shown in Tables 3 and 4, mode shapes, frequencies and modal masses were well preserved by the RM up to Mode #8. As a result, the proposed tailoring of the PS was able to reproduce the dynamic characteristics of the piping system.

4. Model reduction

Let us first establish the system of equations of motion of the piping system subjected to seismic loading where, for simplicity, linear models are assumed. Hence, the dynamic problem can be stated for both PDT and RT cases, respectively, as follows

$$\left(\mathbf{M}^N + \mathbf{M}^P\right)\cdot\ddot{\mathbf{u}} + \mathbf{K}^N\cdot\mathbf{u} = \mathbf{r}^{PDT} + \mathbf{f} \tag{7}$$

$$\mathbf{M}^N\cdot\ddot{\mathbf{u}} + \mathbf{K}^N\cdot\mathbf{u} = \mathbf{r}^{RT} + \mathbf{f} \tag{8}$$

where, M and K stands for mass and stiffness matrices of the system, respectively; u and $\ddot{\mathbf{u}}$are displacement and acceleration vectors; f and r are the external force vector and restoring force vector. For simplicity, damping contributions were neglected in these expressions. In detail, each matrix can be partitioned in pure Numerical-, pure Physical- and Boundary-DoFs, respectively, after Shing (2008). For brevity, the following simplified notation holds: N-DoFs, P-DoFs and B-DoFs, respectively. Thus

$$\mathbf{u} = \begin{bmatrix}\mathbf{u}^{N^T} & \mathbf{u}^{B^T} & \mathbf{u}^{P^T}\end{bmatrix}^T \tag{9}$$

Accordingly, a generic load vector **f** for a typical seismic input reads

$$\mathbf{f} = \begin{bmatrix}\mathbf{f}^{N^T} & \mathbf{f}^{B^T} & \mathbf{f}^{P^T}\end{bmatrix}^T = -\left(\mathbf{M}^N + \mathbf{M}^P\right)\cdot\mathbf{I}\cdot\ddot{u}_g \tag{10}$$

in which,I defines a Boolean vector that projects seismic inertial acceleration $\ddot{u}_g$ to desired DoFs. All matrices must be intended as expanded to the totality of the DoFs of the emulated system being considered. In detail, M and K read, respectively

$$\mathbf{K}^N = \begin{bmatrix} \mathbf{K}_{NN}^N & \mathbf{K}_{NB}^N & \mathbf{0} \\ \mathbf{K}_{BN}^N & \mathbf{K}_{BB}^N & \mathbf{0} \\ \mathbf{0} & \mathbf{0} & \mathbf{0} \end{bmatrix}, \mathbf{K}^P = \begin{bmatrix} \mathbf{0} & \mathbf{0} & \mathbf{0} \\ \mathbf{0} & \mathbf{K}_{BB}^P & \mathbf{K}_{BP}^P \\ \mathbf{0} & \mathbf{K}_{PB}^P & \mathbf{K}_{PP}^P \end{bmatrix}, \qquad \mathbf{M}^N = \begin{bmatrix} \mathbf{M}_{NN}^N & \mathbf{M}_{NB}^N & \mathbf{0} \\ \mathbf{M}_{BN}^N & \mathbf{M}_{BB}^N & \mathbf{0} \\ \mathbf{0} & \mathbf{0} & \mathbf{0} \end{bmatrix}, \mathbf{M}^P = \begin{bmatrix} \mathbf{0} & \mathbf{0} & \mathbf{0} \\ \mathbf{0} & \mathbf{M}_{BB}^P & \mathbf{M}_{BP}^P \\ \mathbf{0} & \mathbf{M}_{PB}^P & \mathbf{M}_{PP}^P \end{bmatrix} \tag{11}$$

Since the restoring force vector r refers to the PS, it is restricted to B- and P-DoFs

$$\mathbf{r} = \begin{bmatrix} \mathbf{0}^T & \mathbf{r}^{B^T} & \mathbf{r}^{P^T} \end{bmatrix}^T \tag{12}$$

In particular, the restoring force vector r is peculiar of the testing strategy and for a linear regime reads

$$\mathbf{r}^{PDT} = -\mathbf{K}^P \cdot \mathbf{u} \tag{13}$$

$$\mathbf{r}^{RT} = -\mathbf{K}^P \cdot \mathbf{u} - \mathbf{M}^P \cdot \ddot{\mathbf{u}} \tag{14}$$

In order to provide reduced matrices and compatible loading vectors, two reduction techniques were analysed and applied herein. They relied on

$$\mathbf{u} = \begin{bmatrix} \mathbf{u}^{N^T} & \mathbf{u}^{B^T} & \mathbf{u}^{P^T} \end{bmatrix}^T = \mathbf{T} \cdot \begin{bmatrix} \mathbf{u}^{N^T} & \mathbf{u}^{B^T} & \mathbf{u}^{q^T} \end{bmatrix}^T \tag{15}$$

whereT is a reduction basis that keeps both N-DoFs and B-DoFs whilst discards remainder P-DoFs. In order to retain important properties of the PS, e.g., mode shapes of interest, further q-DoFscan be introduced. Resulting reduced matrices and vectors read

$$\tilde{\mathrm{K}} = \mathrm{T}^{\mathrm{T}}\mathrm{KT};\ \ \tilde{\mathrm{M}} = \mathrm{T}^{\mathrm{T}}\mathrm{MT};\ \ \tilde{\mathrm{f}} = \mathrm{T}^{\mathrm{T}}\mathrm{f} \tag{16}$$

where $\tilde{\mathrm{K}}, \widetilde{\mathrm{M}}$ and $\tilde{\mathrm{f}}$ represent reduced stiffness matrix, mass matrix and force vector, respectively. From a hybrid simulation perspective, T establishes a kinematic relationship between displacements experienced by retained DoFs, i.e., B-DoFs and q-DoFs, and displacement experienced on discarded DoFs, i.e., P-DoFs. Based on Eq. (16), both (7) and (8) can be condensed.

Reduction strategies entail some general questions: i) how can the minimum rank of an effective reduction basis be estimated? ii) Is there an optimal kinematic relationship, which provides an optimal reduction basis? iii) Which kinematic relationships actually hold for a PS and are they peculiar of the testing strategy? iv) Can a consistent hybrid simulation be performed when the kinematic relationships imposed by the testing procedure are far from those corresponding to the optimal reduction basis? In order to answer to the above-mentioned questions, the Principal Component Analysis (PCA) was of valuable help (Chatterjee 2000).

The PCA is a numerical procedure aimed at projecting a set of possibly correlated vectors into a reduced set of linearly uncorrelated vectors, named Principal Components, which carry the most of the variance of the original vector set. In order to find out the Principal Components of a displacement response X of the PS, the Singular Value Decomposition factorization was applied, i.e.

$$\mathbf{X} = \mathbf{U}\mathbf{S}\mathbf{V}^{T} \tag{17}$$

where: each row of X corresponds to a time history at one node of the PS; each column corresponds to a snapshot of the system at a specific time; column vector u_i of the orthonormal matrix U is the Principal Components of X; column vector v_i of the orthonormal matrix V provides time modulation of corresponding Principal Components u_i; S is a rectangular matrix that contains singular values σ_i of each Principal Component as main diagonal entries in decreasing order. The square of σ_i is the variance carried by X in the Principal Component u_i according to its time modulation v_i; it is proportional to the signal energy of X associated with each Principal Component u_i. The number of non-zero singular values equals the rank of the X matrix. Accordingly, the PCA was applied to the PS, to estimate the minimum rank of suitable reduction bases.

In the present case, X contains discrete values and the PCA is equivalent to the Proper Orthogonal Decomposition. In particular, X collected the displacement responses of the B-DoFs and of the P-DoFs calculated by means of a time history analysis of the RM subjected to selected earthquakes. Let $\sigma_1 > \sigma_2 > \ldots > \sigma_i$ be the decreasing singular values of the dynamic response; if we define $\boldsymbol{E} = \sum_{i=1}^{M} \boldsymbol{\sigma_{ii}}$ as the total energy in the data, $\boldsymbol{E_p} = \sum_{i=1}^{p} \boldsymbol{\sigma_{ii}} / \boldsymbol{E}$represents the normalized data energy carried by the first *p* modes. In this respect, Fig. 7 shows calculated values of E_p up to the 5th proper mode. It can be observed that almost the total energy of data was carried by two main modes, i.e., the Principal Components. On the basis of (17), the data set X was reconstructed by exploiting an increasing number *p* of modes; thus both NEEs and NRMSEs were calculated on coupling Nodes, see Tables 6 and 7, with respect to the RM solution.

Table 6 NEE of reconstructed displacement responses of coupling DoFs with respect to the RM solution

	Number of proper modes retained				
Coupling DoF	1	2	3	4	5
#1	0.0721	0.0086	0.0013	0.0000	0.0000
#2	0.3162	0.0000	0.0000	0.0000	0.0000

Table 7 NRMSE of reconstructed displacement responses of coupling DoFs with respect to the RM solution

	Number of proper modes retained				
Coupling DoF	1	2	3	4	5
#1	0.0353	0.0121	0.0047	0.0001	0.0000
#2	0.0962	0.0000	0.0000	0.0000	0.0000

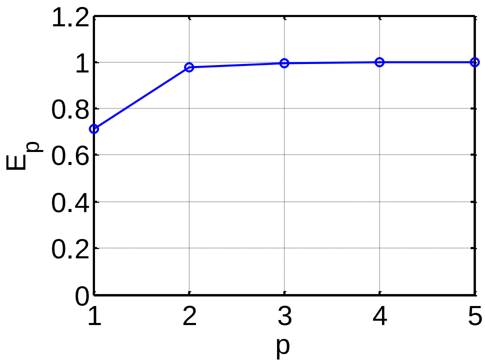

Fig. 7 Cumulative distribution of data energy

A reader can observe that both errors drop after the 2nd proper mode. As a result, the response path of the PS followed a two-dimensional state space path. In addition, answers to the previously posed questions could be: i) a kinematic relationship based on a two rank reduction basis can effectively reduce the PS; ii) an optimal reduction basis should embed the span of principal components. Nonetheless, actual kinematic assumption peculiar of each single testing procedure not necessarily fulfil this requirement, since they depend on the loading excitation; iii) in the case of a real-time interaction between PS and NS, the dynamic properties of the actual autonomous system are preserved in the laboratory; as a result, the SEREP reduction basis was applied to the RT case without adding any further q-DoF (O'Callahan *et al*. 1989). Conversely iv), since the PS could experience only static deformations in the laboratory during PDT, the Craig-Bampton (CB) (1968) approach was selected; as a result, additional q-DoFs, which numerically accounted for non-negligible local dynamics, enriched the Guyan reduction basis(1965).

A preliminary investigation of reduction strategies was conducted in the linear regime. Therefore, both the SEREP and the CB reduction strategies were validated through numerical simulations on the RM of the elastic piping system. The transfer systems– hydraulic actuators – were characterized by an ideal unitary transfer function, i.e. in absence of delay, phase lags and amplitude distortions.

4.1 A modified version of the SEREP method applied to RT

In the RT technique, the PS behaves as a black-box and measured restoring forces can be defined as in Eq. (14).In this case, the SEREP technique was very effective for the reduction of earthquake forces (10) to coupling Nodes. In the ideal case, the coupled system is expected to behave as the emulated piping network, and therefore, modal properties should be preserved. As a consequence, a modified version of the SEREP method, called M-SEREP, was applied. In detail, the eigenvectors of the PS were reduced on a few significant eigenmodes of the global emulated system. In particular, let us split the mass normalized eigenvectors $\mathbf{\Phi}$ of the global emulated system in retained $\mathbf{\Phi}_R$ and truncated $\mathbf{\Phi}_L$ eigenmodes -column wise- and relevant N-DoFs, B-DoFs and P-DoFs -row wise-

$$\mathbf{\Phi} = [\mathbf{\Phi}_R \quad \mathbf{\Phi}_L] = \begin{bmatrix} \mathbf{\Phi}_{RN} & \mathbf{\Phi}_{LN} \\ \mathbf{\Phi}_{RB} & \mathbf{\Phi}_{LB} \\ \mathbf{\Phi}_{RP} & \mathbf{\Phi}_{LP} \end{bmatrix} \tag{18}$$

The SEREP transformation entails

$$\begin{bmatrix} \mathbf{u}^{N^T} & \mathbf{u}^{B^T} & \mathbf{u}^{P^T} \end{bmatrix}^T = \mathbf{T}_{SE} \begin{bmatrix} \mathbf{u}^{N^T} & \mathbf{u}^{B^T} \end{bmatrix}^T \tag{19}$$

where, $\boldsymbol{T}_{SE}$ is named as the SEREP transformation matrix defined as

$$\mathbf{T}_{SE} = \begin{bmatrix} \mathbf{I} & \mathbf{I} & \mathbf{\Phi}_{RP}\mathbf{\Phi}_{RB}^{-1} \end{bmatrix}^T \tag{20}$$

The choice of a specific reduced basis should primarily be based on the type of excitation to which the system is subjected. Accordingly, Mode #1 and Mode #2 depicted in Fig. 6, carried most of the modal mass in x direction; thus they were retained for this reduction. The inversion of $\boldsymbol{\Phi}_{RB}$ entailed a predetermined number of retained modes that must be equal to the number of B-DoFs. Hence, a modified RM was set, where the PS was replaced by its reduced counterpart. Relevant NEE and NRMSE errors calculated with respect to the RM on Coupling DoF responses are reported in Table 8.

In addition, Fig. 8 depicts the displacement response of the Coupling DoF #1 of both the RM and the reduced model.

As one may note, the low values of both NEEs and NRMSEs reported in Table 8 as well as time histories, confirm a good agreement between responses; therefore, the M-SEREP reduction approach was effective.

Table 8 NEE and NRMSE between RM and Reduced model

Error Measure	Coupling DoF #1	Coupling DoF #2
NEE	0.133	0.001
NRMSE	0.015	0.002

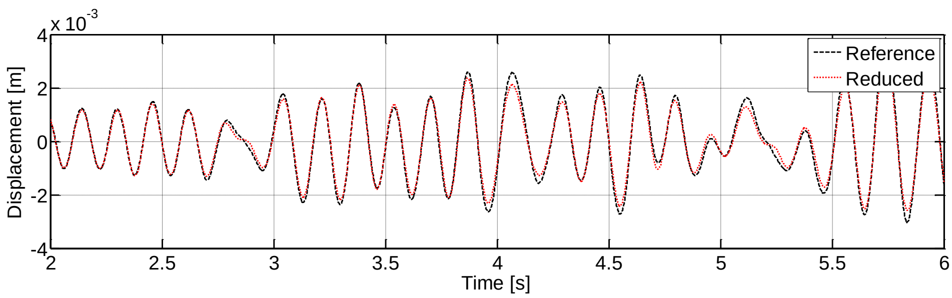

Fig. 8 Comparison of displacement responses of the RM and M-SEREP reduced model at coupling DoF #1

4.2 The Craig-Bampton reduction technique applied to PDT

In order to describe this technique and with reference to the PS, it is necessary to introduce the so-called constraint modes. These modes are static deformation shapes owing to unit displacements applied to boundary DoFs, one by one, whilst the other retained (Girard and Roy 2008). According to their definition, these modes cope with the PDT technique; so, they were calculated through static analyses on the FE model of the PS. Fig. 9 depicts the constraint modes of the PS for both coupling DoFs.

Since the dynamic response of the piping system was described by Modes #1 and #2 depicted in Fig. 6, one can observe that a typical PDT cannot reproduce the response path of the PS. In fact, constraint modes shown in Fig. 9 entail deformations concentrated toward cantilever pipe elements, whilst the remainder parts of the PS remains undeformed. Nonetheless, the portion of the dynamic response of the PS that cannot be excited during the PDT can be simulated numerically. At this point, the Craig-Bampton (CB) method (Craig and Bampton 1968)comes on stage. Starting from the FE model of the PS, its reduced counterpart can be obtained assuming as basis both static and modal vectors, i.e.

$$\mathbf{u} = \begin{bmatrix} \mathbf{u}^N \\ \mathbf{u}^B \\ \mathbf{u}^P \end{bmatrix} = \begin{bmatrix} \mathbf{I} & \mathbf{0} & \mathbf{0} \\ \mathbf{0} & \mathbf{I} & \mathbf{0} \\ \mathbf{0} & \mathbf{\Phi}_S & \mathbf{\Phi}_D \end{bmatrix} \cdot \begin{bmatrix} \mathbf{u}^N \\ \mathbf{u}^B \\ \mathbf{u}^q \end{bmatrix} = \mathbf{T}_{CB} \cdot \begin{bmatrix} \mathbf{u}^N \\ \mathbf{u}^B \\ \mathbf{u}^q \end{bmatrix} = \mathbf{T}_{CB} \cdot \tilde{\mathbf{u}} \tag{21}$$

where, $\boldsymbol{T}_{CB}$ is the CB transformation matrix. With regard to the PS, the matrix $[\mathbf{I} \quad \boldsymbol{\phi}_S]^T$contains the aforementioned constraint modes, whilst $[\mathbf{0} \quad \boldsymbol{\phi}_R]^T$collects a certain number of fixed interface vibration modes. In detail, they correspond to eigenmodes of the substructure constrained at its B-DoFs. The number of constraint modes is fixed and equal to the number of B-DoFs, whilst, the number of fixed interface vibration modes is up to the user. If a proper selection of fixed interface vibration modes is made, a consistent reduced counterpart of the PS valid for both static and dynamic analyses can obtained. Moreover, looking at the block diagonal structure of the reduced stiffness matrix $\widetilde{\mathbf{K}}_{CB}$ provided by (16), i.e.

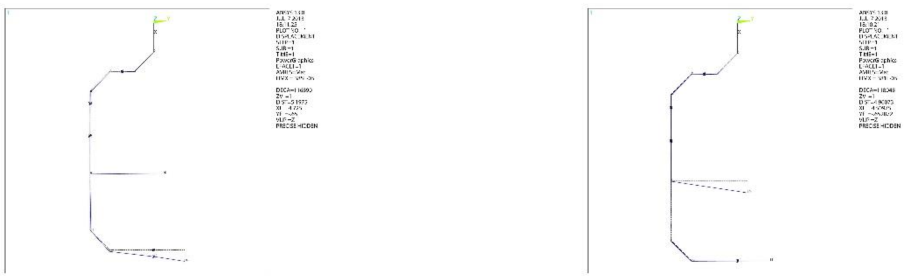

(a) (b)

Fig. 9 (a) Constrained Mode #1; (b) Constrained Mode #2

$$\begin{bmatrix} \mathbf{0} \\ \mathbf{r}^{B} \\ \mathbf{r}^{q} \end{bmatrix} = \begin{bmatrix} \mathbf{0} & \mathbf{0} & \mathbf{0} \\ \mathbf{0} & \mathbf{K}_{BB}^{P,r} & \mathbf{0} \\ \mathbf{0} & \mathbf{0} & \mathbf{K}_{qq}^{P,r} \end{bmatrix} \cdot \begin{bmatrix} \mathbf{u}^{N} \\ \mathbf{u}^{B} \\ \mathbf{u}^{q} \end{bmatrix} \tag{22}$$

the restoring force contribution of constraint and fixed interface vibration modes, one notes that they are pleasantly uncoupled. Since the component $\mathbf{r}^{\boldsymbol{B}}$ is measured during the PDT and the $\mathbf{r}^{\boldsymbol{q}}$ can be easily calculated by the submatrix $\mathbf{K}_{\boldsymbol{qq}}^{\boldsymbol{P,r}}$, the CB method lends itself for an effective implementation of the PDT technique. In order to perform an optimal selection of reduction basis vectors, a sweep analysis was conducted on the number of retained fixed interface vibration modes; they were sorted in decreasing order with respect to their modal masses along the loading direction. For each selection of fixed interface vibration modes, a modified RM embedding the reduced counterpart of the PS was devised and both NEE and NRMSE errors were calculated with respect to the RM on the displacement responses of the Coupling DoFs; they are reported in Tables 9 and 10, respectively.

Table 9 NEEs on coupling DoFs resulting from the sweep analysis

	Number of retained fixed interface vibration modes					
Coupling DoF	0	1	2	3	4	5
#1	0.848	0.012	0.012	0.011	0.011	0.011
#2	0.747	0.015	0.002	0.002	0.002	0.002

Table 10 NRMSEs on coupling DoFs resulting from the sweep analysis

	Number of retained fixed interface vibration modes					
Coupling DoF	0	1	2	3	4	5
#1	0.105	0.006	0.003	0.003	0.003	0.003
#2	0.122	0.003	0.001	0.001	0.001	0.001

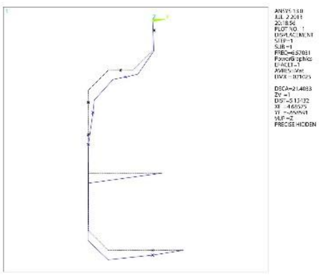

Fig. 10 Fixed Interface Vibration Mode #1 of the PS at 6.57 Hz

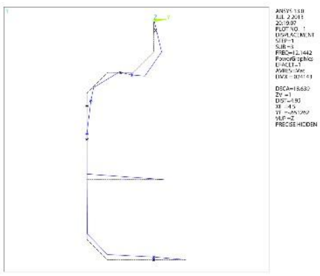

Fig. 11 Fixed Interface Vibration Mode #3 of the PS at 12.44 Hz

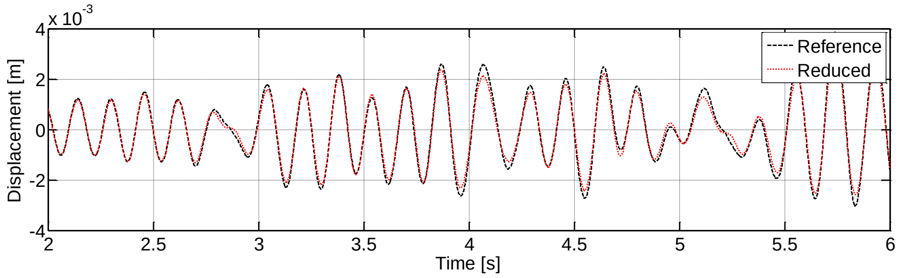

Fig. 12 Comparison of displacement responses of the RM and CB reduced models at coupling DoF #1

On the basis of figures of Table 9 and 10, only two Fixed Interface Vibration Modes #1 and #3 were enough to entail asymptotic values of both NRMSEs and NEEs; these modes are depicted in Figs. 10 and 11 and allowed for a quite accurate reduction.

The dynamic responses of the modified RM embedding the reduced PS with two retained fixed interface vibration modes and of the RM are compared in Fig. 12.

We can conclude that also the CB method allowed for an effective simulation of the piping system by means of PDT techniques.

5. Integration schemes

The robustness and the quality of a PDT or RT depend, among other factors, on the integration scheme employed to solve Eqs. (7) or (8). Since the transfer system is generally affected by delay, distortion of the transfer function and noise, which may lead to instability, unconditionally stable integration methods are preferable, since they are more robust. Typically, real-time machines handling controllers impose a deterministic solving time. Consequently, nonlinear solver characterized by a fixed number of iterations are crucial. Among RT compatible algorithms, the method proposed by Chen and Ricles (2008), the HHT-α implementation of Jung *et al.* (2007) and the "equivalent force control method" of Wu *et al.* (2007) are the most widespread adopted strategies. Nonetheless in hybrid simulations, the numerical models of both NS and PS can be profitably used for dynamic identification, model-based control and/or model order reduction; in these conditions, a unique representation of the system is preferable. As a result, the most flexible and generic state space form represents a reasonable choice. Accordingly, time integration algorithms tailored to first order systems are deemed necessary. Moreover, they allow for the integration of coupled physics characterized by different time derivative orders, e.g., thermo-mechanical coupling. The LSRT-2 algorithm presented hereinafter is conceived for first-order systems, and therefore, fulfils this requirement. In details, it embeds the favourable L-Stability property and is real-time compatible. Moreover, it allowed for time integrating a linear Numerical Substructure characterized by high frequency content with a feasible time step (~1 msec).

In this respect, the following state-space representation is introduced

$$\bar{\mathbf{M}} \cdot \dot{\mathbf{y}}_n + \bar{\mathbf{K}} \cdot \mathbf{y}_n = \mathbf{g}_n \tag{23}$$

where

$$\bar{\mathbf{K}} = \begin{bmatrix} \mathbf{0} & -\mathbf{I} \\ \tilde{\mathbf{K}}^N & \mathbf{0} \end{bmatrix}, \bar{\mathbf{M}} = \begin{bmatrix} \mathbf{I} & \mathbf{0} \\ \mathbf{0} & \tilde{\mathbf{M}}^N \end{bmatrix}, \mathbf{y}_n = \begin{bmatrix} \tilde{\mathbf{u}}_n \\ \tilde{\dot{\mathbf{u}}}_n \end{bmatrix} \ \mathbf{g}_n = \begin{bmatrix} \mathbf{0} \\ \tilde{\mathbf{f}}_n + \tilde{\mathbf{r}}_n^{RT} \end{bmatrix} \tag{24}$$

$$\bar{\mathbf{K}} = \begin{bmatrix} \mathbf{0} & -\mathbf{I} \\ \tilde{\mathbf{K}}^N & \mathbf{0} \end{bmatrix}, \bar{\mathbf{M}} = \begin{bmatrix} \mathbf{I} & \mathbf{0} \\ \mathbf{0} & \tilde{\mathbf{M}}^N + \tilde{\mathbf{M}}^P \end{bmatrix}, \mathbf{y}_n = \begin{bmatrix} \tilde{\mathbf{u}}_n \\ \tilde{\dot{\mathbf{u}}}_n \end{bmatrix} \ \mathbf{g}_n = \begin{bmatrix} \mathbf{0} \\ \tilde{\mathbf{f}}_n + \tilde{\mathbf{r}}_n^{PDT} \end{bmatrix} \tag{25}$$

where, $\mathbf{r}$ is the restoring force vector; Eqs. (24) and (25) refer to the RT and the PDT cases, respectively. To carry out both RTs and PDTs, the L-Stable Real-Time compatible algorithm with two stages (LSRT2) method developed by Bursi *et al.* (2008) was employed. For a proper selection of relevant parameters, this monolithic algorithm results to be second order accurate and L-stable.

The LSRT2 algorithm

The LSRT2 results to be more competitive than popular Runge-Kutta methods in terms of stability, accuracy and ease of implementation (Bursi *et al.* 2008, Bursi *et al.* 2011). This method is unconditionally stable for uncoupled problems and entails a moderate computational cost for real-time performance. It can be summarized in algorithmic form as follows

Stage-1

$$\mathbf{k}_1 = \left(\mathbf{I} - \gamma \cdot \Delta t \cdot \mathbf{J}\right)^{-1} \cdot \left(\bar{\mathbf{M}}^{-1} \cdot \left(\mathbf{g}_n - \bar{\mathbf{K}} \cdot \mathbf{y}_n\right)\right) \cdot \Delta t$$

$$\mathbf{y}_{n+\alpha_2} = \mathbf{y}_n + \alpha_{21} \cdot \mathbf{k}_1$$

where Δt is the time step; the displacement command $\mathbf{y}_{n+\alpha_2}$ is sent to actuators and the restoring force is fed back to the algorithm.

Stage-2

$$\mathbf{k}_2 = \left(\mathbf{I} - \gamma \cdot \Delta t \cdot \mathbf{J}\right)^{-1} \cdot \left(\left(\bar{\mathbf{M}}^{-1} \cdot \left(\mathbf{g}_{n+\alpha_2} - \bar{\mathbf{K}} \cdot \mathbf{y}_{n+\alpha_2}\right)\right) + \mathbf{J} \cdot \gamma_{21} \cdot \mathbf{k}_1\right) \cdot \Delta t$$

$$\mathbf{y}_{n+1} = \mathbf{y}_n + b_1 \cdot \mathbf{k}_1 + b_2 \cdot \mathbf{k}_2$$

The displacement command $\mathbf{y}_{n+1}$ is sent to actuators and the restoring force is fed back to thealgorithm.

In order to preserve A-Stability, the Jacobian matrix $\mathbf{J}$ was evaluated on the global piping system as follows

$$\mathbf{J} = \begin{bmatrix} \mathbf{0} & \mathbf{I} \\ -\left(\tilde{\mathbf{M}}_N + \tilde{\mathbf{M}}_P\right)^{-1} \cdot \left(\tilde{\mathbf{K}}_N + \tilde{\mathbf{K}}_P\right) & -\left(\tilde{\mathbf{M}}_N + \tilde{\mathbf{M}}_P\right)^{-1} \cdot \left(\tilde{\mathbf{C}}_N + \tilde{\mathbf{C}}_P\right) \end{bmatrix} \tag{26}$$

In order to achieve L-stability, second order accuracy and to reduce algorithmic damping in the low frequency range, the following parameters are recommended for the LSRT2 method

$$\gamma = 1 \pm \sqrt{2}/2, \ \alpha_2 = \alpha_{21} = 1/2, \ \gamma_{21} = -\gamma, \ b_1 = 0, \ b_2 = 1$$

Favourable dissipative properties of the LSRT2 are shown in Figs. 13(a) and 13(b), where both the spectral radius ρ and equivalent algorithmic damping $\bar{\xi}$ are depicted. In detail $\Omega = \omega dt$ is the dimensionless frequency and $\Omega = \pi$ corresponds to the normalized Nyquist frequency. Since excitation of higher modes was not appreciated, simulations were conducted considering the less dissipative setting characterized by $\gamma = 1 - \sqrt{2}/2$.

6. Modification of the NS and delay compensation for RT

With regard to RT, a critical limitation was posed by hydraulic actuators. Owing to several factors, such as delay and hydraulic power deficiency, high frequency operations set limits of about +/- 10 mm to maximum strokes of actuators at about 6 Hz. Hence, it was not possible to run an RT on the piping system with high PGA values. Therefore, a modified substructure was conceived by adding masses to several nodes of the NS; thus, the main eigenfrequencies of the piping system were reduced to about 1 Hz. This modifications allowed to carry out RT on the piping system with low PGA earthquakes. This is clear from the test program reported in Table 11. However, note that changes to the NS were conceived towards the development of RT algorithms; they were not intended for improved performance of the piping system at serviceability and/or other limit states.

In order to compensate actuator delays, the over prediction based method developed by Wu *et al.* (2013) was implemented with Simulink (Simulink 2012) models of relevant algorithms. This newly developed compensation technique consists of an upper bound delay τ_c and optimal feedback. It ensures dynamic stability and achieves a nearly exact compensation for delay. The idea behind this over prediction technique is to assume an upper bound delay τ_c not less than the possible maximum delay τ and use it for prediction. The maximum delay of the transfer system was measured through experimental tests of the actuator control system and comparison of the input-output signals; τ_c was taken as 22 ms. The schematic of the over prediction technique is illustrated in Fig. 14.

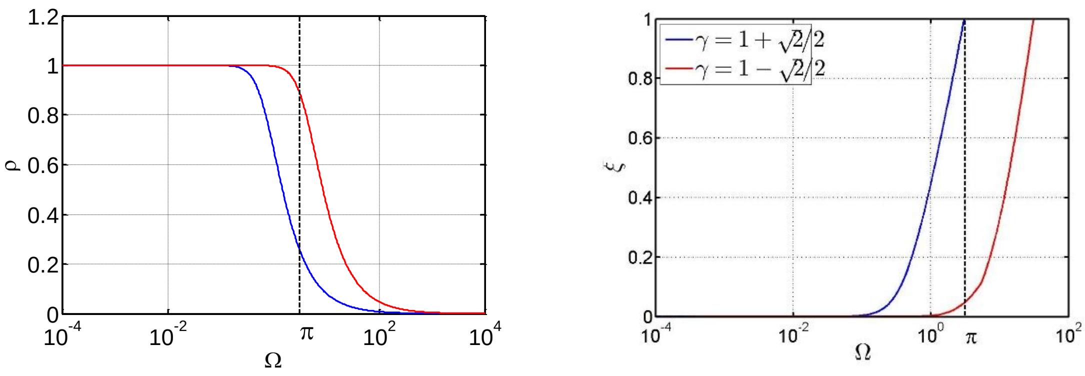

(a) (b)

Fig. 13 (a) Spectral radius ρ and (b) equivalent viscous damping $\bar{\xi}$ relevant to the LSRT2 algorithm

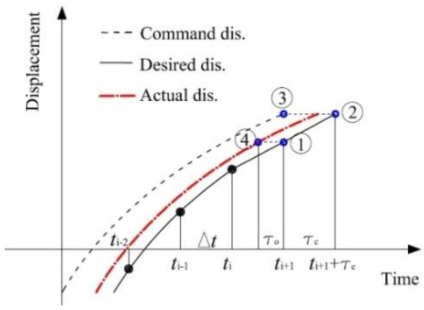

Fig. 14 Schematics of the delay over prediction scheme

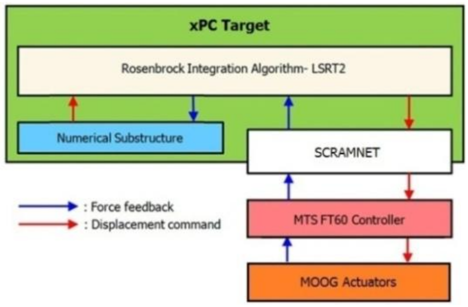

Fig. 15 Hardware-Software architecture

7. Hardware-software configuration

Both mass and stiffness matrices were extracted from a linear elastic FE model of the NS developed in ANSYS FE software. In order to carry out hybrid simulations, those matrices were then used to model the NS by means of the Matlab/Simulink code in the Host PC. The Host PC compiled the system of equations discretized in time by the LSRT2 algorithm, which was then sent to an xPC target -a real time operating system installed in a target PC- via a LAN connection. During experimental tests, integration algorithms solved Eqs. (7) or (8) in the xPC target and estimated displacement commands for the PS. These displacement commands were written to the xPC target, which instantaneously copied these signals to an MTS controller (MTS, 2008) through a SCRAMNET -a reflective memory between the Host PC and the controller-. The controller then commanded two MOOG actuators -capacity: 1000kN force, +/- 250 mm stroke- to move the coupling DoFs to desired positions. Again, the SCRAMNET memory instantaneously supplied corresponding restoring forces measured by load cells to the xPC target. The hardware-software scheme used for hybrid tests is sketched in Fig. 15.

8. Test program and experimental set-up

As reported in Table 11, a number of PDT and RT were carried out. RT were conducted with low PGA values and handled a similar structure owing to limitations underlined in Section 6. PDTs were performed with the CB reduction, while both the M-SEREP and CB reductions were adopted to perform RT. All PDTs were carried out at a 50 times extended earthquake time. In addition to hybrid tests, four Identification Tests (IDTs) were performed on the PS to characterize both its modal properties and damping ratios. In all tests, earthquake loading was applied in the horizontal x direction shown in Fig. 1(b). Note that support motions were not required to be considered separately in hybrid simulations; in fact the system of Eqs. (7) and (8)allowed for relative movements between floor and piping network.

The experimental set-up was placed on the reaction floor of the Materials and Structural Testing laboratory (LPMS) of the University of Trento. The test specimen corresponded to the PS described in Section 3; schematic of the specimen and set-up is depicted in Fig. 16.

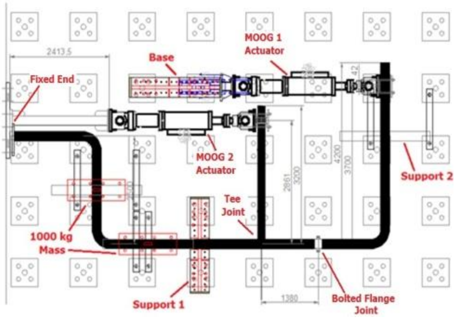

Fig. 16 Schematic of the test set-up

Table 11 Hybrid test program

Test Case				Floor PGA (g)
Identification tests	IDT	-	Hammer Test	-
Real time tests	RT	M-SEREP + LSRT2	RT	0.02
Elastic tests	Elastic test, ET	CB + LSRT2	PDT	0.04
Serviceability limit state tests	Operational limit state test, SLOT	CB + LSRT2	PDT	0.08
	Damage limit state test, SLDT	CB + LSRT2	PDT	0.11
Ultimate limit state tests	Safe life limit state test, SLVT	CB + LSRT2	PDT	0.42
	Collapse limit state test, SLCT	CB + LSRT2	PDT	0.60

In order to measure strains, displacements and rotations in different positions, the test specimen and in particular, elbows and the Tee joint, were instrumented with 22 strain gauges and 7 displacement transducers. Data were acquired by 4 Spider8 acquisition systems and by an MTS FT60 controller. IDTs were carried out using 10 accelerometers and a National Instruments data acquisition system.

9. Main experimental results and validation of test algorithms

All hybrid simulations listed in Table 11 were successfully carried out. A 0.5% damping found through the IDTs was used in the NS during tests. Experimental results exhibited a favourable performance of the piping system and its components under all limit state earthquakes. In fact, it was observed that, even under SLC, the whole piping system remained below its yield limits without any leakage, and only limited strains and rotations were found in different components. In all tests, maximum strain was found in Elbow #2, as can be noted in Fig. 17(a); in greater detail, the maximum elbow flank strain at SLCT was about 950 μm/m, which was well below its yield strain of 2019 μm/m.

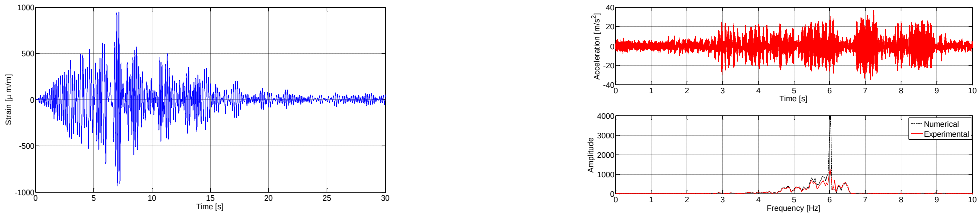

(a) (b)

Fig. 17 (a) Strain histories in Elbow #2 and (b) acceleration history and relevant spectra of Coupling DoF #1 at SLCT

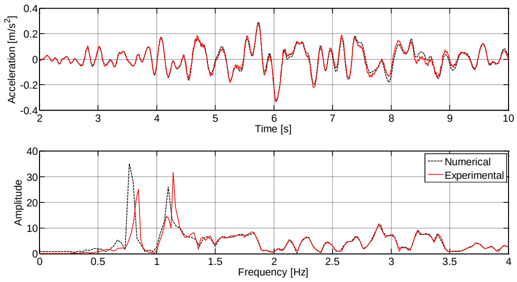

Fig. 18 Accelerations of Coupling DoF #2 forRT

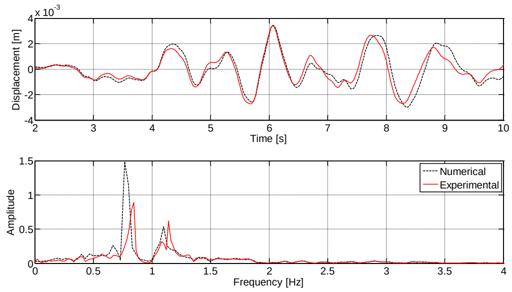

Fig. 19 Displacements of Coupling DoF #2 for RT

Fig. 17(b) presents acceleration time history of Coupling DoF #1 at SLCT. One can observe that the input earthquake at 5.88 m/s^2 was significantly amplified during testing; in fact, the maximum acceleration was about twice that of the corresponding input. Moreover, relevant Fourier spectra illustrate that the dynamic response of the piping system was dominated by its lower modes corresponding to 5.87 Hz -1st Mode-and 6.32 Hz -2nd Mode-.

With regard to RTDS, the piping system exhibited a favourable response. See in this respect, the acceleration time history of Coupling DoF #2 from RT presented in Fig. 18. One may note that the input PGA was amplified about three times in this test. Moreover, relevant Fourier spectra show that the system's responses were dominated by its lower modes corresponding to frequencies

0.78 Hz and 1.10 Hz. In addition, the LSRT2 integrator proved to be effective for RT; as depicted in Fig. 19, it entailed experimental responses in agreement with relevant numerical simulations.

Because the PS responded in the linear range, both NEE and NRMSE errors were quantified also for these cases. Relevant estimates can be found in Tables 12 and 13 for PDT and RT, respectively.

Given the different approximations involved, NRMSE error values indicated a favourable agreement between numerical and experimental results. As expected and because of signal energy involved, NEE errors were found to be comparatively greater. Thus, effectiveness of both the CB and M-SEREP reduction techniques were experimentally justified as was predicted analytically. Moreover, a favourable performance of the piping system was found, which always remained in the linear regime without any leakage; thus the over-conservativeness of relevant design standards was confirmed (Touboul *et al.* 2006, Otani *et al.* 2011, Paolacci *et al.* 2011, 2013b). In addition, the choice of reduction bases derived from a linear FE model of the piping system was supported.

Table 12 NEE and NRMSE between experimental and numerical responses in the PDT case at SLCT

Error	Coupling DoF #1	Coupling DoF #2
NEE	0.236	0.635
NRMSE	0.038	0.066

Table 13 NEEs and NRMSEs between experimental and numerical responses in the RT case

Error	Coupling DoF #1	Coupling DoF #2
NEE	0.494	0.614
NRMSE	0.083	0.239

10. Conclusions

This paper presented a novel hybrid testing approach for seismic performance evaluation of industrial piping systems based on model reduction techniques. In this respect, a deep insight into the dynamic response of an emulated global system from a specimen perspective was provided, by means of the application of principal component analysis. The clear understanding of reduction basis requirements paved the way for the implementation of two model reduction techniques aimed at extending the applicability range of hybrid testing techniques beyond its traditional scope. In detail, a modified version of the SEREP method was applied to the Real Time testing strategy, whilst the well-known Craig-Bampton method was tailored to the Pseudo-Dynamic Testing case. Numerical and experimental validations of the proposed approaches were presented throughout the paper in terms of two error measures capable of emphasizing both energy and frequency aspects involved in approximations.

With regard to time integration, the LSRT2 algorithm tailored to Hamiltonian system was adopted in the experimental campaign. The relevant state-space form naturally favour the exploitation of a more general framework where numerical integration, model reduction, system identification and control techniques can more easily interact, As a result, both the Real Time and the Pseudo-Dynamic Testing techniques were successfully applied to the suggested case study. The favourable performance of the piping system, which always remained in the linear regime without any leakage, corroborated the choice of reduction bases derived from linear time-invariant FE models. Hence, the reduction techniques involved in hybrid testing presented in this study proved to be justified. The enhancement of reduction techniques to nonlinear PSs will represent its natural extension.

Acknowledgments

The work presented herein was carried out with a financial grant from the European Union through the INDUSE project (Grant No. RFSR-CT-2009-00022). Moreover, support of the European research project SERIES (Grant number: 227887) is also greatly acknowledged. Finally, we thank Dr. Nie and Dr. Hofmayer from Brookhaven National Laboratory for the provision of some earthquake records.

References

ANSYS (2007), *Release 11.0 documentation for ANSYS*, Online Manual, ANSYS, Inc.

Braconi, A., Bursi, O.S., Fabbrocino, G., Salvatore, W. and Tremblay, R. (2008a), "Seismic performance of a 3D full-scale high-ductility steel-concrete composite moment-resisting structure - part I: design and testing procedure", *Earthq. Eng. Struct. D.*, **37**(14), 1609-1634.

Braconi, A., Bursi, O.S., Fabbrocino, G., Salvatore, W., Taucer, F. and Tremblay, R. (2008b), "Seismic performance of a 3D full-scale high-ductile steel-concrete composite moment-resisting frame - part II: test results and analytical validation", *Earthq. Eng. Struct. D.*, **37**(14), 1635-1655.

Bursi, O.S., Buelga, A.G., Vulcan, L., Neild, S.A. and Wagg, D.J. (2008), "Novel coupling Rosenbrock-based algorithms for real-time dynamic substructure testing", *Earthq. Eng. Struct. D.*, **37**, 339-360.

Bursi O.S., Wagg D.J.E. (Eds.) (2008), *Modern Testing Techniques for Structural Systems*, CISM International Centre for Mechanical Sciences, **502**, Springer, Vienna.

Bursi, O.S., Jia, C., Vulcan, L., Neild, S.A. and Wagg D.J. (2011), "Rosenbrock-based algorithms and subcycling strategies for real-time nonlinear substructure testing", *Earthq. Eng. Struct. D.*, **40**(1), 2011, 1-19.

Chatterjee, A. (2000), "An introduction to the proper orthogonal decomposition", *Curr. Sci.*, **78**, 808-817.

Chen, C. and Ricles, J.M. (2008), "Development of direct integration algorithms for structural dynamics using discrete control theory", *J. Eng. Mech. - ASCE*, **134**(8), 676-683, doi:10.1061/(ASCE)0733-9399 (2008)134:8(676).

Chrysostomou, C.Z., Poljansek, M., Kyriakides, N., Taucer, F. and Molina, F.J. (2013), "Pseudo-dynamic tests on a full-Scale four-storey reinforced concrete frame seismically retrofitted with reinforced Concrete infilling", *Struct. Eng. Int.*, **23**(2), 159-166.

Craig, R. and Bampton, M. (1968), "Coupling of substructures for dynamic analysis", *AIAA J.*, **6**(7), 1313-1319.

DeGrassi, G., Nie, J. and Hofmayer, C. (2008), "Seismic analysis of large-scale piping systems for the JNES-NUPEC ultimate strength piping test program", U.S. NRC. NUREG/CR-6983, BNL-NUREG-81548-2008.

De Melo, F.J.M.Q., Carneiro, J.A.O., Lopes, H.R., Rodrigues, J.F.D. and Gomes, J.F.S. (2001), "The dynamic analysis of piping systems using pseudo-dynamic Techniques", *J. Strain Anal. Eng.*, **36** (5), 441-451.

EN 13480-3(2002), Metallic industrial piping - Part 3: Design and calculation.

Girard A. and Roy N. (2008), *Structural Dynamics in Industry*, ISTE/Hermes Science Publishing.

Guyan, R.J. (1965), "Reduction of stiffness and mass matrices", *Am. Inst. Aeronaut. Astronaut. J.*, **3**(2), 380.

Hibbit, H.D., Karlsson B.I. and Sorensen (2003), "Theory Manual, ABAQUS, version 6.3", Providence, RI. USA.

Horiuchi, T., Inoue, M., Konno, T. and Namita, Y. (1999), "Real-time hybrid experimental system with actuator delay compensation and its application to a piping system with energy absorber", *Earthq. Eng. Struct. D.*, **28**(10), 1121–1141.

Jung, R., Shing, P.B., Stauffer, E. and Thoen, B. (2007), "Performance of a real-time pseudo dynamic test system considering nonlinear structural response", *Earthq. Eng. Struct. D.*, **36**, 1785-1809.

Klerk, D., Rixen, D.J. and Voormeeren, S.N. (2008), "General framework for dynamic substructuring: history, review and classification of techniques", *AIAA J.*, **46**(5), 1169-1181. doi:10.2514/1.33274.

Krausmann, E., Cruz, A.M. and Affeltranger, B. (2010), "The impact of the 12 May 2008 Wenchuan earthquake on industrial facilities", *J. Loss Prevention in the Process Industries*, **23**(2), 242-248.

Mahin, S.A. and Shing, P.B. (1985), "Pseudo dynamic method for seismic testing", *J. Struct. Eng. -ASCE*, **111**(7), 1482-1503.

Ministere de l'ecologie du developpement durable des transports et du logement (2011), "Arrete du 24 janvier 2011 fixant les regles parasismiques applicables a certaines installations classes, DEVP1102251A, *Journal Official de la RepubliqueFrancaise*. Texte 14 sur 239.

MTS (2008), *Models FlexTest 40/60/100/200 Controller Hardware*, MTS Systems Corporation.

NormeTechniche (2008*), Norme Techniche per le costruzioni*, DM Infrastrutture.

O'Callahan, J.C. (1989a), "A new procedure for and improved reduced system IRS", *In IMAC VII*, Las Vegas.

O'Callahan, J.C., Avitabile, P. and Riemer, R. (1989b), "System equivalent reduction expansion process (SEREP)", *Proceedings of the 6th International Modal Analysis Conference*, Las Vegas, January.

Otani, A., Nakamura, I., Takada, H. and Shiratori, M. (2011), "Consideration on seismic design margin of elbow in piping", *Proceedings of the ASME 2011 Pressure Vessels 237 and Piping Division Conference, PVP2011*, July 17-21, 2011, Baltimore, Maryland, USA.

Paolacci, F., Reza, M.S. and Bursi, O.S. (2011), "Seismic design criteria of refinery piping systems", *Proceedings of the COMPDYN 2011-III ECCOMAS Thematic Conference on Computational Methods in Structural Dynamics and Earthquake Engineering*, Corfu, Greece, 26-28 May.

Paolacci, F., Giannini, R. and Angelis, M.D. (2013a), "Seismic response mitigation of chemical plant components by passive control systems", *J. Loss Prevention in Process Industries*, DOI:10.1016/j.jlp.2013.03.003.

Paolacci, F., Reza, M.S., Bursi, O.S., Gresnigt, N. and Kumar, A. (2013b), "Main issues on the seismic design of industrial piping systems and components", *Proceedings of the ASME 2013 Pressure Vessels & Piping Division Conference, PVP 2013*, July 14-18, 2013, Paris, France.

Pastor, M., Binda, M. and Harčarik, T. (2012), "Modal Assurance Criterion", *Procedia Eng.*, **48**, 543-548, http://dx.doi.org/10.1016/j.proeng.2012.09.551.

Reza, M.S., Bursi,O.S., Paolacci, F. and Kumar, A. (2014), "Enhanced seismic performance of non-standard bolted flange joints for petrochemical piping systems", *J. Loss Prevention in the Process Industries*, **30**, 124-136.

Saouma V. and Sivaselvan M.V. (eds) (2008), *Hybrid simulation: Theory, implementation and applications*, Taylor & Francis.

Shing, P.B., Nakashima, M. and Bursi, O.S. (1996), "Application of pseudo dynamic test method to structural research", *Earthq. Spectra, EERI*, **12**(1), 29-54.

Shing, P.B. (2008), “Real-time hybrid testing techniques” in *Modern testing techniques for structural systems* (Eds., Bursi, O.S. and Wagg, D.J.E.), CISM International Centre for Mechanical Sciences, Springer, Vienna.

Simulink v 8.0 (2012), The Math Works, Inc.

Touboul, F., Blay, N., Sollogoub, P. and Chapuliot, S. (2006), “Enhanced seismic criteria for piping”, *Nuclear Eng. Design*, **236**, 1-9.

Vervaeck, A. and Daniell J. (2012), “Japan -366 days after the Quake… 19000 lives lost, 1.2 million buildings damaged, $574 billion”, *Earthquake-Report.com*, http://earthquake-report.com/2012/03/10/ japan-366-days-after-the-quake-19000-lives-lost-1-2-million -bui ldings-damaged-574-billion/

Varelis, G.E., Karamanos, S.A. and Gresnigt, A.M. (2012), “Pipe elbows under strong cyclic loading”, *J. Pressure Vessel Technol*., **135**(1), 011207-011207-9. doi:10.1115/1.4007293.

Wallace, M.I., Wagg, D.J., Neild, S.A., Bunniss, P., Lieven, N.A.J. and Crewe, A.J. (2007), “Testing coupled rotor blade–lag damper vibration using real-time dynamic substructuring”, *J. Sound Vib*., **307**(3-6), 737-754.

Wu, B., Wang, Q., Shing, P.B. and Ou, J. (2007), “Equivalent force control method for generalized real-time substructure testing with implicit integration”, *Earthq. Eng. Struct. D.*, **6**(9), 1127-1149.

Wu, B., Wang, Z. and Bursi, O.S. (2013), “Actuator dynamics compensation based on upper bound delay for real-time hybrid simulation”, *Earthq. Eng. Struct. D.*, doi: 10.1002/eqe.2296.

Yoshihiko, T. (2012), “Study on analogy between dynamic load and displacement-controlled load”, *Int. J. Pressure Vessels Piping*, **90-91**, 37-45.

Zare, M.R. and Wilkson, S. (2010), “Resilience of wastewater pipelines in earthquakes”, *Proceedings of the* 9^{th} *U.S. National and* 10^{th} *Canadian Conference*, Toronto, Ontario, Canada, 25-29 July.